Enhanced Photocatalytic Degradation of Ciprofloxacin over $Bi_2O_3/(BiO)_2CO_3$ Heterojunctions: Efficiency, Kinetics, Pathways, Mechanisms and Toxicity Evaluation

Meijuan Chen, Jie Yao, Yu Huang, Han Gong, Wei Chu

PII: S1385-8947(17)31777-1
DOI: https://doi.org/10.1016/j.cej.2017.10.064
Reference: CEJ 17848

To appear in: *Chemical Engineering Journal*

Received Date: 1 July 2017
Revised Date: 28 September 2017
Accepted Date: 13 October 2017

Please cite this article as: M. Chen, J. Yao, Y. Huang, H. Gong, W. Chu, Enhanced Photocatalytic Degradation of Ciprofloxacin over $Bi_2O_3/(BiO)_2CO_3$ Heterojunctions: Efficiency, Kinetics, Pathways, Mechanisms and Toxicity Evaluation, *Chemical Engineering Journal* (2017), doi: https://doi.org/10.1016/j.cej.2017.10.064

Enhanced Photocatalytic Degradation of Ciprofloxacin over $Bi_2O_3/(BiO)_2CO_3$ Heterojunctions: Efficiency, Kinetics, Pathways, Mechanisms and Toxicity Evaluation

Meijuan Chen[1,2], Jie Yao[2], Yu Huang[2,3], Han Gong[4], Wei Chu[4]*

1. *School of Human Settlements and Civil Engineering, Xi'an Jiaotong University, Xi'an 710049, China*
2. *Key Lab of Aerosol Chemistry & Physics, Institute of Earth Environment, Chinese Academy of Sciences, Xi'an 710061, China*
3. *State Key Lab of Loess and Quaternary Geology (SKLLQG), Institute of Earth Environment, Chinese Academy of Sciences, Xi'an 710061, China*
4. *Department of Civil and Environmental Engineering, The Hong Kong Polytechnic University, Hung Hom, Kowloon, Hong Kong 999077, China*

*Corresponding author: Prof. Yu Huang

E-mail address: huangyu@ieecas.cn

Tel: +86-02962336261

Fax: +86-02962336261

Abstract

In this study, the degradation of antibiotic ciprofloxacin (CIP) over $Bi_2O_3/(BiO)_2CO_3$ heterojunctions under simulated solar light irradiation (SSL-$Bi_2O_3/(BiO)_2CO_3$) was examined for the first time. The results showed that the $Bi_2O_3/(BiO)_2CO_3$ heterojunctions dramatically improved CIP decay efficiency. The effect of parameters showed that the CIP decay was optimized with the $Bi_2O_3/(BiO)_2CO_3$ dosage of 0.5 g/L and a wide pH range of 4.0-8.3, based on which, a kinetic model was derived to predict the remaining CIP concentration. It was found that the presence of anions like SO_4^{2-}, NO_3^- and HCO_3^- decelerated the CIP decay, while the co-existence of Cl^- accelerated the CIP decay. Six degradation intermediates were identified by ultra-performance liquid chromatography coupled with mass analyzer (UPLC/MS) and ion chromatographic (IC) analysis, and the decay pathways and degradation mechanism of CIP were proposed by combining the experiment data with theoretical calculation of frontier electron densities. Hydroxyl radical's reaction, photo-hole (h^+) oxidation and reductive defluorination were found to involve in the CIP decay. The efficient alleviation on total organic carbon (TOC) and toxicity indicated that the complete mineralization and de-toxicity are possible by this system with sufficient reaction time.

Keywords: $Bi_2O_3/(BiO)_2CO_3$; Ciprofloxacin; Kinetics model; Degradation mechanism; Toxicity

1. Introduction

Antibiotics, as one of the largest groups of PPCPs (pharmaceuticals and personal care products), has recently received intensive attention [1]. For example, ciprofloxacin (CIP) is a typical broad spectrum antibiotic and has been popularly used as human and veterinary medicine [2]. Since about 50% of the oral dose is excreted unchanged in the urine with 24 h thus producing high urinary concentrations [3], it subsequently enters the WWTPs (waste water treatment plants). It was reported that ciprofloxacin is detected in both influent and effluent of WWTPs [4], the effluent subsequently enters the aqueous environment and results in the frequent detection in groundwater, surface water, sewage water and seawater throughout the world [5-7]. CIP is found in surface water at levels up to 13 ng/L in Germany [8], while 0.03 μg/L of CIP has been detected in U.S. streams [9]. In China, the CIP pollution reaches up to 3.35, 5.93 and 2.10 μg/L in animal farm-effluent, river and pond water, respectively [10]. Previous literatures reveal that the occurrence of CIP at trace level (ng/L) gives birth to antibiotic resistant bacteria [11] and resistance genes [4], which should further impair the selection of genetic variants of microorganisms and imposes adverse effect on human health [12, 13]. Thereby, the CIP removal from water environment attracts more and more attentions [14-16].

Conventional methods, like sewage treatment plants and biological degradation cannot remove CIP efficiently because of the bio-resistant property of CIP [17]. Therefore, it is highly desired for developing efficient and environmental friendly approaches to remove CIP. In recent years, advanced oxidation processes (AOPs) such as chlorination [18], ozonation [19] and permanganate oxidation [20] have been reported to be efficient in CIP degradation. However, the selectivity of radicals in these AOPs restrain the complete mineralization of organic pollutants [21]. As a comparison, the non-selective hydroxyl radical (•OH) is promising for complete mineralization by converting organic compounds into CO_2 and mineral acids [21]. Moreover, The •OH radical always involves in a fast mineralization with the rate constant 2-4 orders of magnitude higher than that of chlorination, ozonation and permanganate oxidation [21]. Bismuth subcarbonate $(BiO)_2CO_3$) as an environmental

friendly photocatalyst has received increasing interest because it can oxidize lots of organic molecules by producing •OH radicals [22]. Nevertheless, the photocatalytic performance of $(BiO)_2CO_3$ is in need of improving because it can only be excited by ultraviolet light (with a large band gap of *ca.* 3.4 eV). Up to date, many attempts have been made to fabricate new $(BiO)_2CO_3$ photocatalysts by coupling it with smaller band gap semiconductors to construct extended optical absorption. The $(BiO)_2CO_3$-based heterojunctions like $Bi_2S_3/(BiO)_2CO_3$ [23], $BiOI/(BiO)_2CO_3$ [24] and $Bi/(BiO)_2CO_3$ [25] have been successfully fabricated with high photocatalytic performance. In our previous study, a $Bi_2O_3/(BiO)_2CO_3$ heterojunction has been prepared by a facile one-step thermal-treatment approach, which has been confirmed that •OH radicals dominates the photocatalytic reaction under solar light irradiation [26, 27].

However, the application of $Bi_2O_3/(BiO)_2CO_3$ heterojunction regarding to the effect of field parameters is still limited, especially in lacking of predicting mathematic model, which are critical in achieving effective operational parameters for further industrial optimization. Moreover, the occurrence and fate of byproducts/intermediates is of significance because the byproducts/intermediates are different from the parent compounds in not only the chemical and physical properties but also the toxicity [28]. For instance, Richard and coworker found that the oxidation of antibiotic ciprofloxacin by UV/H_2O_2 in pure water lead to the formation of cytotoxic by-products [29]. Our previous study found that the harmful intermediates were formed in the early stage of antibiotics norfloxacin degradation over Bi_2WO_6 photocatalyst [30]. Therefore, to clarify the occurrence and fate of by-products is an essential prerequisite for building a safety treatment process.

In this study, the as-prepared $Bi_2O_3/(BiO)_2CO_3$ heterojunction was employed to degrade antibiotic ciprofloxacin in aqueous solution under simulated solar light irradiation (SSL-$Bi_2O_3/(BiO)_2CO_3$). To the best of our knowledge, this is the first time to apply $(BiO)_2CO_3$-based heterojunction for aqueous ciprofloxacin decay. Field parameters, like the CIP concentration, $Bi_2O_3/(BiO)_2CO_3$ dosage and pH level were investigated and optimized. A predicting kinetics model was derived thereby. The

aromatic intermediates and inorganic byproducts were identified. The decay pathways and degradation mechanism of CIP were proposed by combining the experiment data with theoretical calculation of frontier electron densities. TOC and antibacterial activity were examined.

2. Experimental

2.1 Materials

Ciprofloxacin ($C_{17}H_{18}FN_3O_3$, abbreviated as CIP) from Sigma-Aldrich company was used as the probe in this study. $Bi_2O_3/(BiO)_2CO_3$ heterojunction was prepared using bismuth nitrate ($Bi(NO_3)_3$, Sigma-Aldrich) and urea ($CO(NH_2)_2$, Sinopharm Chemical Reagent Company) as precursors. The preparation method has been stated in our previous study [26]. In brief, 10 mmol of $CO(NH_2)_2$ and 2.5 mmol of $Bi(NO_3)_3$ powders were mixed in 35 mL distilled deionized water. The mixture was transferred into autoclave, then moved to the muffle furnace at 160 °C for 12 h. After which, a white $(BiO)_2CO_3$ sample was obtained. To obtain the $Bi_2O_3/(BiO)_2CO_3$ composites, the $(BiO)_2CO_3$ sample was treated by calcining at 400 °C. For comparison, the Bi_2O_3 sample was prepared by increasing the calcination temperature to 500 °C.

Acetonitrile (Tedia Company) and distilled-deionized water were used for mobile phase for high-performance liquid chromatography (HPLC) analysis. The distilled-deionized water was obtained from a pure water treatment system (Bamstead NANO, USA). The formic acid (HCOOH) and orthophosphoric acid (H_3PO_4) were used for pH adjustment in mobile phase (Sigma-Aldrich). Other chemicals like sodium nitrate ($NaNO_3$), sodium sulfate (Na_2SO_4), sodium bicarbonate ($NaHCO_3$), sodium chloride (NaCl), hydrochloric acid (HCl) and sodium hydroxide (NaOH) were all purchased from Sigma-Aldrich Company.

2.2 Characterization

The diffuse reflectance spectrum of catalysts were recorded on the UV visible spectrophotometer (U-4100, Hitachi). A Bruker Electron spin resonance (ESR) spectroscopy was used to detect •OH and $•O_2^-$ radicals (ER200-SRC). Transmission

electron microscopy (TEM) pictures were performed on a JEOL electron microscope (JEM-2010). The Brunauer-Emmett-Teller (BET) surface area was examined by an ASAP 2020 N-adsorption apparatus. The effective diameter of catalyst and zeta potential of catalysts were tested with Zeta potential measurement analyzer (Colloidal Dynamics, USA). The effective diameter was tested in distilled-deionized water and it represented the real particle size after dispersing in aqueous solution.

2.3 Photocatalytic activity evaluation

The degradation of ciprofloxacin was carried out in a photochemical reactor under simulated solar light irradiation (PLS-SXE 300, Beijing Changtuo). The light was supplied by a 300 W Xenon lamp and the light intensity was set at 0.641w/cm^2. Before the reaction, a predetermined amount of photocatalyst and 100 mL ciprofloxacin solution were added into a quartz beaker, and stirred for 30 min in darkness to achieve adsorption equilibrium (See Figure S1). After which, the reaction was started by igniting the pre-heated light. During the reaction, an aliquot (1 mL) sample was withdrawn from the solution at preset intervals. In order to remove the solid matters and facilitate the further analysis, the withdrawn sample was filtrated through a PTFE (polytetrafluoroethylene) membrane with a pore diameter of 0.2 μm. All degradation experiments were tested at room temperature of 23 ± 1 ^{o}C (air-conditioned). Parts of degradation experiments were tested in triplicated and the standard deviations were less than 7% (See Figure S2).

2.4 Analytical methods of degradation intermediates and final products

The residual ciprofloxacin was determined by an Agilent 1200 series High Performance Liquid Chromatography (HPLC) with a diode array detector. A Restek C18 column was used to separate ciprofloxacin and its intermediates (5.0 μm, 4.6 × 250 mm). The adsorption wavelength of HPLC was set at 272 nm. The mobile phase was prepared by mixing 20 mM H_3PO_4 solution and acetonitrile with a volume ratio of 1:4. The absorption spectra of CIP from High Performance Liquid Chromatography were shown in Figure S3. The time-dependent peak area of CIP was summarized in

Table S1.

The organic intermediates were identified by a Dionex UltiMate 3000 ultra-performance liquid chromatography (UPLC) equipment with a Bruker ion trap mass analyzer at the positive ion mode. A Thermo C8 column (1.9 μm, 50 lumn on was used to separate the intermediates. The mobile phase for LC/MS analysis was composed by (A) acetonitrile and (B) 0.1% formic acid solution (in volume) and run at a flow rate of 1 mL/min. The mobile phase was changed by the following gradient: 100% of B was linearly decreased to 40% during the first 2 min; The mixture of 40% of B and 60% of A kept constant from 2 to 20 min; from 20 to 22 min, A was continuously linearly increased from 60% to 100%.

The produced inorganic byproducts during the reaction were investigated by a Dionex 4500i ion chromatography. The Dionex anion column (IonPac AS14, 4 mm × 250 mm) and the anion column (Dionex IonPac AS14, 4 mm × 250 mm) were used for anion and cation analysis, respectively. The flow rates were both set as 1 mL/min. The mobile phase for anion analysis was a mixture of 3.5 mM Na_2CO_3 and 1 mM $NaHCO_3$, while the 0.022 M methanesulfonic acid solution was used for cation analysis. A Shimadzu Total organic carbon (TOC) analyzer was used to examine the TOC removal.

2.5 Calculation of frontier electron densities of CIP

The Gaussian 09 program was employed to calculate the frontier electron densities of the atoms in FLU molecule at the B3LYP/6-311G** level. During the calculation, water was chosen as the solvent. The values of $2FED^2_{HOMO}$ were used to predict the initial sites for electron extraction (e.g. photo generated h^+ reaction) on CIP molecule, while $FED^2_{HOMO}+FED^2_{LUMO}$ indicated the initial sites for hydroxyl addition.

2.6 Toxicity evaluation

The toxicity of CIP and its degradation products was examined by plate count method using *Escherichia coli* as reference microorganism. The assays were carried out by dispersion 50 μL of bacterial suspension and 50 μL of the treated samples on the

surface of agar plate. The plates were then incubated at 37 ^{o}C for 18 h. The number of survived colonies was counted. Each test was carried out in triplicated and the mean values were used. The toxicity was calculated by the following equation:

$$Toxicity = (1 - \frac{survived\ colonies\ of\ samples}{raw\ colonies}) \times 100\%.$$

The raw colonies represent the survived colonies by dispersion 50 μL of bacterial suspension without the addition of sample.

3. Results and discussion

3.1. The decay of CIP over different catalysts

Figure 1a displayed the CIP decay over $Bi_2O_3/(BiO)_2CO_3$, Bi_2O_3 and $(BiO)_2CO_3$ under simulated solar light irradiation. The process with sole simulated solar light irradiation (SSL) was investigated for comparison. As shown in Figure 1a, a decay performance of 60.7% was achieved by direct SSL photolysis in 30 min, which was probably initiated by absorbing photon at a given wavelength to reach the excited state of CIP [31]. In the presence of photocatalysts, the CIP decay followed the order of $Bi_2O_3/(BiO)_2CO_3$ > Bi_2O_3 > $(BiO)_2CO_3$, where the removal efficiency achieved 93.4%, 86.5% and 77.9% in 30 min, respectively. This phenomenon is in agreement with the results of light absorption (Figure 1b) and ESR analysis (Figure 1c). Both absorption edge and the intensity of •OH radicals showed the same order to CIP decay with $Bi_2O_3/(BiO)_2CO_3$ > Bi_2O_3 > $(BiO)_2CO_3$, where the absorption edge of $Bi_2O_3/(BiO)_2CO_3$, Bi_2O_3 and $(BiO)_2CO_3$ is 570, 470 and 380 nm, respectively, while the ESR analysis showed that the intensity of •OH signal was the highest in $Bi_2O_3/(BiO)_2CO_3$. The broader light absorption leads to more photons absorbed by photocatalyst, and results in more active radicals (i.e. •OH radicals) and better photocatalytic performance [32]. Moreover, the heterojunction interface in $Bi_2O_3/(BiO)_2CO_3$ (Figure 1d) should benefit the performance because the interface could efficiently enhance the separation of photo-generated e^--h^+ pairs and speed up the interfacial charges transferring rate to adsorbed substrates [26]. In addition, the highest surface area and smallest effective diameter of $Bi_2O_3/(BiO)_2CO_3$ as shown in

Table 1 were promoters for its highest performance: The high surface area facilitates the diffusion of CIP and active radicals [33]; The smallest effective diameter of $Bi_2O_3/(BiO)_2CO_3$ in aqueous suspension suggested the $Bi_2O_3/(BiO)_2CO_3$ owned the best dispersion among the three catalysts, which accelerated the CIP decay by allowing more photons adsorbed on the catalyst surface and benefiting the contact between pollutant's molecule and photocatalyst [34].

3.2. Effect of different parameters, including $[CIP]_0$, $[Bi_2O_3/(BiO)_2CO_3]_0$ and pH_0

The CIP decay in the SSL-$Bi_2O_3/(BiO)_2CO_3$ system by varying $[CIP]_0$ (initial CIP concentration) was shown in Figure 2. The CIP decay followed pseudo-first-order kinetics, and presented a rate constant (k) of 0.090, 0.101, 0.128, 0.294 and 0.476 min^{-1} for $[CIP]_0$ at 1, 3, 5, 8 and 10 mg/L, respectively. It can be seen that higher $[CIP]_0$ resulted in lower CIP decay efficiency. Possible explanations for this observations were: (1) with the increase of $[CIP]_0$, more photons were absorbed by CIP, which subsequently reduced the portion for $Bi_2O_3/(BiO)_2CO_3$ photocatalysis [35]; (2) some byproducts/intermediates were produced in CIP decay, which was excepted to increase with the increment of $[CIP]_0$, resulting in the competitive reactions between $\bullet OH$ radicals and byproducts [36]. The heterogeneous photocatalytic reaction was usually described by a Langmuir-Hinshelwood (LH) model as shown below:

$$\frac{1}{k} = \frac{1}{k_{LH}}[CIP]_0 + \frac{1}{k_{LH}K_L} \quad (1)$$

where k is the observed pseudo-first-order rate constant (min^{-1}), k_{LH} is the apparent rate constant of the reaction occurring on the $Bi_2O_3/(BiO)_2CO_3$ heterogeneous surface ($mM \cdot min^{-1}$), and K_L (mM^{-1}) is the equilibrium adsorption constant of CIP onto the $Bi_2O_3/(BiO)_2CO_3$ surface. By linear regression the data of k and $1/[CIP]_0$, a fine r^2 level of 0.92 was achieved (as shown in the inset of Figure 2), which suggested that the experimental results fitted well with the LH model. This obsevation confirmed that the CIP degardation was a heterogeneous reaction, which dominatly occured on the $Bi_2O_3/(BiO)_2CO_3$ surface in the SSL-$Bi_2O_3/(BiO)_2CO_3$ system [30].

The influence of initial $Bi_2O_3/(BiO)_2CO_3$ dosage ($[Bi_2O_3/(BiO)_2CO_3]_0$) on the CIP decay was studied as $[Bi_2O_3/(BiO)_2CO_3]_0$ changed from 0 to 0.8 g/L. The experimental results were illustrated in Figure 3. It was observed that the k value increased linearly with the increment of $[Bi_2O_3/(BiO)_2CO_3]_0$ and reached the optimum value as $[Bi_2O_3/(BiO)_2CO_3]_0$ = 0.5 g/L. After which, the k value was declined. As shown in the inset of Figure 3, the k curve was clearly divided into two linear stages at the breakpoint of 0.5 g/L. The proportional increment of the suspended amount of $Bi_2O_3/(BiO)_2CO_3$ at the beginning could increase the yield of active radicals and the number of reaction sites [37]. As a result, the k value was linearly increased with $[Bi_2O_3/(BiO)_2CO_3]_0$ at 0 - 0.5 g/L, suggesting that any dosage at 0 - 0.5 g/L is acceptable since equal amout of $Bi_2O_3/(BiO)_2CO_3$ shows equal performance. The further increase of $[Bi_2O_3/(BiO)_2CO_3]_0$ would induce the self-scavenging of the excesss •OH radicals (Eq. 2) [38].

$$\cdot OH + \cdot OH \rightarrow H_2O_2 \quad (2)$$

In addition, the overdose of $Bi_2O_3/(BiO)_2CO_3$ resulted in the increase of light opacity and the reduction of light penetration [39]. In another word, the endless increase of $Bi_2O_3/(BiO)_2CO_3$ dosage will not guarantee a fast CIP decay.

The influence of the intial pH level (pH_0) on CIP decay was investigated. As depicted in Figure 4, the CIP decay was largely pH-dependent, and the decay rate k reached 0.060, 0.117, 0.105, 0.100 and 0.042 at pH_0 of 3.0, 4.0, 5.9, 8.3 and 10.3, respectively. The insert of Figure 4 showed variation trends of the k value at different pH levels. It can be observed that the k value ascended from pH 3.0 to 4.0, and reached an optimal level at pH 4.0, after which the k value almost kept constant between pH 4.0 and 8.3, and then decreased with the further increment of pH level. It was known that there are four pKa values of CIP, i.e. pKa_1 = 3.64, pKa_2 = 5.05, pKa_3 = 5.86-6.35, pKa_4 = 8.24-8.95 [40] (see in Figure S4), meanwhile, the point of zero charge (PZC) of $Bi_2O_3/(BiO)_2CO_3$ was determined to be pH = 9.2 (see in Figure 5). These observations indicated that the surface charge of CIP and $Bi_2O_3/(BiO)_2CO_3$ would be greatly affected by the solution pH. At pH 3.0, the CIP molecule was

protonated since the four pka values of CIP were all higher than 3.0, whereas the surface of $Bi_2O_3/(BiO)_2CO_3$ was positively charged (see Figure 5). As a result, the electrostatic repulsion between positive charges of CIP and $Bi_2O_3/(BiO)_2CO_3$ made the adsorption of CIP onto the $Bi_2O_3/(BiO)_2CO_3$ surface quite difficult, which results in the restrained CIP decay. The optimum CIP decay at the wide pH range of 4.0-8.3 could be attributed to the electroneutral property of CIP. It can be determined from Figure S4 that the CIP molecule contained both positive and negative charges concurrently at the pH period of 4.0-8.3 [40], thereby, it can approach to the positively charged $Bi_2O_3/(BiO)_2CO_3$ easily by electrostatic attraction. A sharp k decrease at pH 10.3 was attributed to the electrostatic repulsive between CIP and $Bi_2O_3/(BiO)_2CO_3$ since they were both negatively charged. It deserved to note that the working pH for $Bi_2O_3/(BiO)_2CO_3$ is broad at pH 4.0-8.3, which fully covers the environmental tolerance pH of wastewater (6.0-8.0) [41]. Therefore, the $Bi_2O_3/(BiO)_2CO_3$ is a promising photocatalyst for CIP decay in wastewater.

3.3 Kinetics model for the remaining concentration of CIP

To build a cost-effective system, it is necessary to determine the proper catalyst dosage, operating pH level, CIP concentration as well as reasonable reaction time. The experiment results showed that the rational $Bi_2O_3/(BiO)_2CO_3$ dosage was below 0.5 g/L and the optimum pH level was located at 4.0-8.3. Therefore, the kinetic model was derived at $[Bi_2O_3/(BiO)_2CO_3]_0$ < 0.5 g/L and pH = 4.0-8.3 for the SSL-$Bi_2O_3/(BiO)_2CO_3$ system.

It was found that for all $[CIP]_0$ levels, $[Bi_2O_3/(BiO)_2CO_3]_0$ < 0.5 g/L and pH = 4.0-8.3, the k (min^{-1}) value was linearly related to $1/[CIP]_0$ (L/mg), $[Bi_2O_3/(BiO)_2CO_3]_0$ (g/L) and pH, as shown in the inset images in Figure 2, 3 and 4, respectively.

In details, from the inset of Figure 2, the k was correlated to the $1/[CIP]_0$ like Eq. 3.

$$k = 0.4226\frac{1}{[CIP]_0} + 0.0713 \quad (3)$$

For $[Bi_2O_3/(BiO)_2CO_3]_0$ < 0.5 g/L, the k was predictable as indicated in Eq. 4.

$$k = 0.1123[Bi_2O_3/(BiO)_2CO_3]_0 + 0.0407 \quad (4)$$

In addition, it was depicted in Figure 4 that the k values almost keep constant around 0.9999 at pH 4.0-8.3, the k could be described by following Eq.5.

$$k = 0 \times pH + 0.9999 \quad (5)$$

It is feasible in theory to integrate above three linear relations (Eq. 3, 4 and 5) into one simple equation. After a multiple linear regressions, the integrated equation can be expressed as Eq. 6.

$$k = 0.1397[Bi_2O_3/(BiO)_2CO_3]_0 + 0.4314\frac{1}{[CIP]_0} - 0.0036pH + 0.0143 \quad (6)$$

It was noted that the pH coefficient of 0.0036 is close to 0, which was consistent with that the pH level kept constant at pH 4.0-8.3 as described in Eq. 5. As a result, the pH effect at 4.0-8.3 was ignorable, and the predicting formula could be re-regressed by Eq. 7.

$$k = 0.1379[Bi_2O_3/(BiO)_2CO_3]_0 + 0.4324\frac{1}{[CIP]_0} - 0.00541 \quad (7)$$

The remaining concentration of CIP can be predicted by the pseudo-first-order kinetics as shown in Eq. 8.

$$C = C_0 \times e^{-kt} \quad (8)$$

where C and C_0 represent the remaining and initial concentration of CIP, respectively (both with the unit of mg/L), k is the observed pseudo-first-order rate constant (min^{-1}) and t is the reaction time (min).

After incorporating Eq. 7 into Eq. 8, the remaining concentration of CIP can be predicted by the following equation,

$$C = C_0 \times e^{-(0.1379[Bi_2O_3/(BiO)_2CO_3]_0 + 0.4324\frac{1}{[CIP]_0} - 0.00541)t} \quad (9)$$

The CIP decay data and predicting curves were compared in Figure 6. It can be found that the predicting curves fitted well to the original data, which suggested that the proposed kinetics model was successful for predicting the remaining CIP within the test conditions.

3.4 Effect of anions

The CIP decay was investigated with the addition of inorganic anions such as Cl^-, NO_3^-, HCO_3^- and SO_4^{2-}. The results in Figure 7 showed that SO_4^{2-}, NO_3^- and HCO_3^- retarded the CIP decay, while Cl^- accelerated the decay. The adverse impact of SO_4^{2-} might be ascribed to the following equation [42],

$$SO_4^{2-} + \cdot OH \rightarrow \cdot SO_4^- + H_2O \qquad (10)$$

The SO_4^{2-} anion can be converted to a weaker oxidizing agent of sulfate radical ($\bullet SO_4^-$) by the consumption of •OH radicals. It is known that the $\bullet SO_4^-$ radical is of selectivity and presents a big molecule structure as compared with •OH radicals, which provides less chance for reacting with pollutant [43].

The HCO_3^- was reported to be the •OH radical scavenger as stated in Eq. 11 [44]. Similar to $\bullet SO_4^-$, the formed $\cdot HCO_3$ is a weaker and selective radicals, which restrains the CIP decay.

$$HCO_3^- + \cdot OH \rightarrow \cdot HCO_3 + H_2O \qquad (11)$$

Liu et al. pointed out that the NO_3^- showed inappreciable influence on the degradation of organic pollutants in the •OH dominating process [38]. Differently, an apparently inhibition effect was found in this study. It should be ascribed to the presence of N atoms in CIP molecule, where the N atom in organic pollutant was reported to be oxidized to NO_3^- by the attack of •OH radicals, as seen in Eq. 12 [45]. The yield of NO_3^- may decrease the decay rate of CIP in view of the Equlibrium Law (Le Chatelier's principle).

$$\text{CIP}\left(\begin{array}{c}|\\ -\text{N}-\end{array}\right) + \cdot OH \rightarrow NO_3^- \qquad (12)$$

It can be seen from Eq. 13-14 that the Cl^- anion can react with •OH radicals to form $\bullet HOCl^-$, and subsequently transform into $\bullet Cl$ [46].

$$Cl^- + \cdot OH \rightarrow \cdot HOCl^- \qquad (13)$$

$$\cdot HOCl^- + H^+ \rightarrow \cdot Cl + H_2O \qquad (14)$$

The generated secondary oxidants of $\bullet HOCl^-$ and $\bullet Cl$ were both effective in organic pollutants degradation [47, 48], which offered parallel pathways for CIP and resulted in an accelerated CIP decay.

3.5 Reaction mechanism

In order to identify CIP byproducts/intermediates, the intermediates generating from SSL-Bi_2O_3/$(BiO)_2CO_3$ photocatalysis were identified by LC/MS. Six intermediates were identified for CIP decay in the system. The molecular structure of intermediates was identified by the MS spectrum in Figure S5-S11. The intermediates properties including the molecular weight of pronated ion ($[M+H^+]$) and molecular structure were summarized in Table S2. It can be judged from the intermediates structure that the CIP decay should be originated from two paths, i.e. piperazine oxidation and reductive defluorination.

Figure 8 depicted the accumulation profiles of CIP and intermediates plotting as the normalized peak areas against irradiation time. The piperazine ring open was believed to be one of the major primary byproducts, because the intermediates originated from piperazine ring open, e.g. I_1 and I_2, were formed at the begginning and gradually accumulated up to the maximum amount at 1.5 h, then declined at the end of the run. The intermediate I_3 should be the subsequent byproducts because it still stayed at the accumulation stage at the end of the run despite it appeared at the beginning of the process. The intermediates I_4 and I_5 arose at the middle of the process (0.3 and 0.5 h respectively) and accumulated at the end of the run, indicating they are later byproducts.

The reaction sites on CIP were also estimated by the calculation of frontier electron densities. The calculating results were list in Table 2, and the site of CIP atom was labeled in Figure S12. According to frontier orbital theory, the atom with a higher value of $FED^2_{HOMO}+FED^2_{LUMO}$ is the preferential position for hydroxyl radicals, while the atom with a higher $2FED^2_{HOMO}$ stands for the position where the electron can be easily extracted, e.g. the direct h^+ reaction in photoctalysis. For the hydroxyl radical's reaction, the first reaction site was predicted based on the values of $FED^2_{HOMO}+FED^2_{LUMO}$. N24 was found to be the highest value of $FED^2_{HOMO}+FED^2_{LUMO}$, indicating that N24 should be the first site for hydroxyl radical's attacking. N23 should be the second site for hydroxyl radical attack in view

of its second largest FED^2_{HOMO}+FED^2_{LUMO} value. As shown in the CIP decay pathways in Figure 9. The intermediate I_1 with $[M+H^+]$ = 362 should be attributed to the piperazine oxidation, where N24 and N23 in piperazine ring were attacked by •OH radicals, resulting in the yield of two aldehyde groups. Similar reaction between piperazine and •OH radicals was reported in TiO_2 photocatalysis [49]. The further •OH oxidation on N24 and then N23 may result in the rearrangement and decarbonylation with the generation of intermediates $[M+H^+]$ = 334 and 306, respectively. Besides hydroxyl radicals' attack, photo h^+ oxidation are usually presented in photocatalytic process [50]. The first addition position of the h^+ probably took place on the position of the highest $2FED^2_{HOMO}$. N24 and N23 were found to be the first and second reaction site for photo h^+ as shown in Table 2. It can be deduced that the intermediates $[M+H^+]$ = 334 and 306 can also obtained from photo h^+ reaction on N24 and N23, respectively, resulting from the continuous decarbonylation reactions. The decarbonylation reaction route and corresponding intermediates were detected in the Bi_2WO_6 photocatalytic degradation of piperazine ring [42]. However, neither of intermediate $[M+H^+]$ = 334 nor 306 was detected by the LC/MS analysis. The absence of compounds with $[M+H^+]$ 334 and 306 in this study might be ascribed to its short lifetime with fast transferring rate to later intermediates. Apparently, the I_2 came from the reductive defluorination at I_1, where the reductive defluorination should be ascribed to the photolysis since similar reaction was found in CIP photolysis [51], rather than the •OH radicals reaction [52]. The intermediate I_3 with $[M+H^+]$ = 316, for 28 Da and 18 Da lower than the molecular ion of I_2 and compound $[M+H^+]$ 334, theoretically are formed by the decarbonylation (on N24 and/or N23) and reductive defluorination, respectively. Similarly, the intermediates I_4 with $[M+H^+]$ = 288 came from the reductive defluorination of compound $[M+H^+]$ 306 and the decarbonylation of I_3. The intermediates I_5 with $[M+H^+]$ = 263, for 43 Da lower than the $[M+H^+]$ 306, should be originated from the loss of $–C_2H_5N$ fragment. The intermediates I_6 should be ascribed to the reductive defluorination of I_5 and the loss of $–C_2H_5N$ fragment of I_4. The loss of $–C_2H_5N$ fragment is attributed to the photo h^+ oxidation on the N23 position.

Figure 10 showed the accumulation profiles of inorganic ions at predetermined time intervals. It can be seen that the fluoride (F^-), ammonium (NH_4^+) and nitrate (NO_3^-) ions were gradually increased in the process. Agreement with the decay routes in Figure 9, the F^- apparently derived from defluorination. The NH_4^+ and NO_3^- ions are resulted from the nitrogen loss at piperazine ring. The NH_4^+ ion was detected in the piperazine ring destruction in our previous Bi_2WO_6 photocatalysis [42]. The NO_3^- should be ascribed to the further oxidation of NH_4^+ by ·OH attack (see Eq. 15) [45].

$$NH_4^+ + \cdot OH \rightarrow NO_3^- \quad (15)$$

However, the NO_3^- was absence at the piperazine ring destruction via our Bi_2WO_6 photocatalysis [42], because the pollutant and its daughter intermediates are competitors of NH_4^+ for ·OH radicals, therefore only abundant ·OH radicals can initiate the NH_4^+ oxidation [30]. The detection of NO_3^- in this study suggests that the ·OH radicals generating from $Bi_2O_3/(BiO)_2CO_3$ photocatalysis is of abundance. In addition, the detection of NO_3^- in the byproducts is in coincidence with above finding that the addition of NO_3^- into the system inhibited the CIP decay.

3.6 Mineralization and toxicity evaluation

Mineralization of ciprofloxacin by $Bi_2O_3/(BiO)_2CO_3$ photocatalysis was estimated by measuring the TOC content of the reaction solutions. As shown in Figure 11, although the mole balance reduction of ciprofloxacin was nearly 90%, the TOC removal was only 21%. That is because the aliphatic intermediates generated from the ring-opening reaction might be more resistant towards further mineralization as reported by Oturan [53]. Nevertheless, complete mineralization of CIP by the SSL-$Bi_2O_3/(BiO)_2CO_3$ system is possible if sufficient reaction time is provided.

E. Coli was used as reference organism for the estimation of the residual toxicity of CIP and its intermediates. The typical results were presented in Figure 11, where the toxicity was almost unchanged in first the 1.5 h, and subsequently it was graduate decreased. At the end of 2.5 h treatment, the toxicity decreased to 39.4%, suggesting the effective elimination of toxicity of CIP and the intermediates by the SSL-$Bi_2O_3/(BiO)_2CO_3$ system.

Moreover, the stability of the $Bi_2O_3/(BiO)_2CO_3$ heterojunction in degrading CIP under identical conditions was evaluated by the cyclic degradation experiments presented in Figure S13. The decay efficiency shows an almost imperceptible decrease with a decline of 5.2% after 5 times runs, suggesting that the $Bi_2O_3/(BiO)_2CO_3$ heterojunction possessed good stability in this system.

Conclusions

In this study, the decay kinetics and degradation mechanism of antibiotic CIP by SSL-$Bi_2O_3/(BiO)_2CO_3$ system were investigated for the first time. The $Bi_2O_3/(BiO)_2CO_3$ showed better performance than that of pristine $(BiO)_2CO_3$ and Bi_2O_3. The CIP decay followed a pseudo-first-order kinetics, where the rate constant k increased with the decreasing of the initial CIP concentration. The CIP decay was optimized at [$Bi_2O_3/(BiO)_2CO_3$] = 0.5 g/L and pH levels at 4.0-8.3. A prediction model was derived based on the rational experimental conditions, and the proposed model fitted well to the original data. The inorganic anions of SO_4^{2-}, NO_3^- and HCO_3^- retarded the CIP decay, while Cl^- slightly improved the destruction of CIP. The degradation intermediates were identified by UPLC/MS and IC analysis. The decay pathways and degradation mechanism of CIP were proposed by combining the experiment data with theoretical calculation of frontier electron densities. Hydroxyl radical's reaction, photo-hole (h^+) oxidation and reductive defluorination were found to involve in the CIP decay. The efficient alleviation on total organic carbon (TOC) and toxicity indicated that the complete mineralization and de-toxicity are possible by this system with sufficient reaction time. This study provides useful information for the real application of this system in aquatic environment.

Acknowledgment

This research was financially supported by the National Natural Science Foundation of China (41503102), the China Postdoctoral Science Foundation (2015M572568), Shaanxi Postdoctoral Science Foundation (2016BSHEDZZ35) and the National Key Research and Development Program of China (2016YFA0203000). Yu Huang is also

supported by the "Hundred Talent Program" of the Chinese Academy of Sciences.

References:

[1] H. Guo, N. Gao, Y. Yang, Y. Zhang, Kinetics and transformation pathways on oxidation of fluoroquinolones with thermally activated persulfate, Chemical Engineering Journal, 292 (2016) 82-91.

[2] H.A. Duong, N.H. Pham, H.T. Nguyen, T.T. Hoang, H.V. Pham, V.C. Pham, M. Berg, W. Giger, A.C. Alder, Occurrence, fate and antibiotic resistance of fluoroquinolone antibacterials in hospital wastewaters in Hanoi, Vietnam, Chemosphere, 72 (2008) 968-973.

[3] A. Navalón, O. Ballesteros, R. Blanc, J.L. Vílchez, Determination of ciprofloxacin in human urine and serum samples by solid-phase spectrofluorimetry, Talanta, 52 (2000) 845-852.

[4] S. Rodriguez-Mozaz, S. Chamorro, E. Marti, B. Huerta, M. Gros, A. Sànchez-Melsió, C.M. Borrego, D. Barceló, J.L. Balcázar, Occurrence of antibiotics and antibiotic resistance genes in hospital and urban wastewaters and their impact on the receiving river, Water Research, 69 (2015) 234-242.

[5] W. Giger, A.C. Alder, E.M. Golet, H.P.E. Kohler, C.S. McArdell, E. Molnar, H. Siegrist, M.J.F. Suter, Occurrence and fate of antibiotics as trace contaminants in wastewaters, sewage sludges, and surface waters, Chimia, 57 (2003) 485-491.

[6] W.J. Sim, J.W. Lee, J.E. Oh, Occurrence and fate of pharmaceuticals in wastewater treatment plants and rivers in Korea, Environmental Pollution, 158 (2010) 1938-1947.

[7] S.R. Nagulapally, A. Ahmad, A. Henry, G.L. Marchin, L. Zurek, A. Bhandari, Occurrence of Ciprofloxacin-, Trimethoprim-Sulfamethoxazole-, and Vancomycin-Resistant Bacteria in a Municipal Wastewater Treatment Plant, Water Environment Research, 81 (2009) 82-90.

[8] T. Christian, R.J. Schneider, H.A. Farber, D. Skutlarek, M.T. Meyer, H.E. Goldbach, Determination of antibiotic residues in manure, soil, and surface waters, Acta Hydrochimica Et Hydrobiologica, 31 (2003) 36-44.

[9] D.W. Kolpin, E.T. Furlong, M.T. Meyer, E.M. Thurman, S.D. Zaugg, L.B. Barber, H.T. Buxton, Pharmaceuticals, hormones, and other organic wastewater contaminants in US streams, 1999-2000: A national reconnaissance, Environmental Science & Technology, 36 (2002) 1202-1211.

[10] R.C. Wei, F. Ge, M. Chen, R. Wang, Occurrence of Ciprofloxacin, Enrofloxacin, and Florfenicol in Animal Wastewater and Water Resources, Journal of Environmental Quality, 41 (2012) 1481-1486.

[11] E. Gullberg, S. Cao, O.G. Berg, C. Ilback, L. Sandegren, D. Hughes, D.I. Andersson, Selection of Resistant Bacteria at Very Low Antibiotic Concentrations, Plos Pathogens, 7 (2011).

[12] K. Kümmerer, Antibiotics in the aquatic environment – A review – Part I, Chemosphere, 75 (2009) 417-434.

[13] K. Oberlé, M.J. Capdeville, T. Berthe, H. Budzinski, F. Petit, Evidence for a complex relationship between antibiotics and antibiotic-resistant *Escherichia coli*: From medical center patients to a receiving environment, Environmental Science and Technology, 46 (2012) 1859-1868.

[14] V.S. Antonin, M.C. Santos, S. Garcia-Segura, E. Brillas, Electrochemical incineration of the antibiotic ciprofloxacin in sulfate medium and synthetic urine matrix, Water Research, 83 (2015) 31-41.

[15] Y. Hong, C. Li, G. Zhang, Y. Meng, B. Yin, Y. Zhao, W. Shi, Efficient and stable Nb_2O_5 modified g-C_3N_4 photocatalyst for removal of antibiotic pollutant, Chemical Engineering Journal, 299 (2016) 74-84.

[16] Y. Ji, C. Ferronato, A. Salvador, X. Yang, J.-M. Chovelon, Degradation of ciprofloxacin and

sulfamethoxazole by ferrous-activated persulfate: Implications for remediation of groundwater contaminated by antibiotics, Science of the Total Environment, 472 (2014) 800-808.

[17] L.W. Matzek, K.E. Carter, Sustained persulfate activation using solid iron: kinetics and application to ciprofloxacin degradation, Chemical Engineering Journal.

[18] M.C. Dodd, A.D. Shah, U. Von Gunten, C.H. Huang, Interactions of fluoroquinolone antibacterial agents with aqueous chlorine: Reaction kinetics, mechanisms, and transformation pathways, Environmental Science & Technology, 39 (2005) 7065-7076.

[19] A. Tekle-Roettering, K.S. Jewell, E. Reisz, H.V. Lutze, T.A. Ternes, W. Schmidt, T.C. Schmidt, Ozonation of piperidine, piperazine and morpholine: Kinetics, stoichiometry, product formation and mechanistic considerations, Water Research, 88 (2016) 960-971.

[20] Y. Xu, S. Liu, F. Guo, B. Zhang, Evaluation of the oxidation of enrofloxacin by permanganate and the antimicrobial activity of the products, Chemosphere, 144 (2016) 113-121.

[21] V.K. Sharma, T.M. Triantis, M.G. Antoniou, X. He, M. Pelaez, C. Han, W. Song, K.E. O'Shea, A.A. de la Cruz, T. Kaloudis, A. Hiskia, D.D. Dionysiou, Destruction of microcystins by conventional and advanced oxidation processes: A review, Separation and Purification Technology, 91 (2012) 3-17.

[22] A. Umar, R. Ahmad, R. Kumar, A.A. Ibrahim, S. Baskoutas, $Bi_2O_2CO_3$ nanoplates: Fabrication and characterization of highly sensitive and selective cholesterol biosensor, Journal of Alloys and Compounds, 683 (2016) 433-438.

[23] Y. Zhu, D. Xu, M. Meng, Ultrasonic-assisted synthesis of amorphous Bi_2S_3 coupled $(BiO)_2CO_3$ catalyst with improved visible light-responsive photocatalytic activity, Journal of Materials Science, 50 (2015) 1594-1604.

[24] J. Cao, X. Li, H. Lin, S. Chen, X. Fu, In situ preparation of novel p–n junction photocatalyst BiOI/$(BiO)_2CO_3$ with enhanced visible light photocatalytic activity, Journal of Hazardous Materials, 239–240 (2012) 316-324.

[25] F. Dong, Q. Li, Y. Sun, W.-K. Ho, Noble Metal-Like Behavior of Plasmonic Bi Particles as a Cocatalyst Deposited on $(BiO)_2CO_3$ Microspheres for Efficient Visible Light Photocatalysis, ACS Catalysis, 4 (2014) 4341-4350.

[26] Y. Huang, W. Wang, Q. Zhang, J.J. Cao, R.J. Huang, W.K. Ho, S.C. Lee, In situ Fabrication of alpha-Bi_2O_3/$(BiO)_2CO_3$ Nanoplate Heterojunctions with Tunable Optical Property and Photocatalytic Activity, Scientific Reports, 6 (2016).

[27] J. Kuncewicz, P. Ząbek, K. Kruczała, K. Szaciłowski, W. Macyk, Photocatalysis Involving a Visible Light-Induced Hole Injection in a Chromate(VI)–TiO_2 System, The Journal of Physical Chemistry C, 116 (2012) 21762-21770.

[28] M. DellaGreca, A. Fiorentino, M.R. Iesce, M. Isidori, A. Nardelli, L. Previtera, F. Temussi, Identification of phototransformation products of prednisone by sunlight: Toxicity of the drug and its derivatives on aquatic organisms, Environmental Toxicology and Chemistry, 22 (2003) 534-539.

[29] J. Richard, A. Boergers, C. vom Eyser, K. Bester, J. Tuerk, Toxicity of the micropollutants Bisphenol A, Ciprofloxacin, Metoprolol and Sulfamethoxazole in water samples before and after the oxidative treatment, International Journal of Hygiene and Environmental Health, 217 (2014) 506-514.

[30] M. Chen, W. Chu, Efficient Degradation of an Antibiotic Norfloxacin in Aqueous Solution via a Simulated Solar-Light-Mediated Bi_2WO_6 Process, Industrial & Engineering Chemistry Research, 51 (2012) 4887-4893.

[31] Y.Q. Liu, X.X. He, X.D. Duan, Y.S. Fu, D.D. Dionysiou, Photochemical degradation of oxytetracycline: Influence of pH and role of carbonate radical, Chemical Engineering Journal, 276

(2015) 113-121.

[32] Y.K. Huang, S.F. Kang, Y. Yang, H.F. Qin, Z.J. Ni, S.J. Yang, X. Li, Facile synthesis of Bi/Bi_2WO_6 nanocomposite with enhanced photocatalytic activity under visible light, Applied Catalysis B-Environmental, 196 (2016) 89-99.

[33] H. Huang, X. Li, J. Wang, F. Dong, P.K. Chu, T. Zhang, Y. Zhang, Anionic Group Self-Doping as a Promising Strategy: Band-Gap Engineering and Multi-Functional Applications of High-Performance CO_3^{2-}-Doped $Bi_2O_2CO_3$, Acs Catalysis, 5 (2015) 4094-4103.

[34] P. Wilhelm, D. Stephan, Photodegradation of rhodamine B in aqueous solution via $SiO_2@TiO_2$ nano-spheres, Journal of Photochemistry and Photobiology A: Chemistry, 185 (2007) 19-25.

[35] Y. Liu, X. He, X. Duan, Y. Fu, D.D. Dionysiou, Photochemical degradation of oxytetracycline: Influence of pH and role of carbonate radical, Chemical Engineering Journal, 276 (2015) 113-121.

[36] Y. Liu, X. He, Y. Fu, D.D. Dionysiou, Kinetics and mechanism investigation on the destruction of oxytetracycline by UV-254 nm activation of persulfate, Journal of Hazardous Materials, 305 (2016) 229-239.

[37] C. Cai, Z. Zhang, J. Liu, N. Shan, H. Zhang, D.D. Dionysiou, Visible light-assisted heterogeneous Fenton with $ZnFe_2O_4$ for the degradation of Orange II in water, Applied Catalysis B: Environmental, 182 (2016) 456-468.

[38] Y. Liu, X. He, Y. Fu, D.D. Dionysiou, Degradation kinetics and mechanism of oxytetracycline by hydroxyl radical-based advanced oxidation processes, Chemical Engineering Journal, 284 (2016) 1317-1327.

[39] M. Chen, W. Chu, Degradation of antibiotic norfloxacin in aqueous solution by visible-light-mediated C-TiO_2 photocatalysis, Journal of Hazardous Materials, 219 (2012) 183-189.

[40] X. Zhang, R. Li, M. Jia, S. Wang, Y. Huang, C. Chen, Degradation of ciprofloxacin in aqueous bismuth oxybromide (BiOBr) suspensions under visible light irradiation: A direct hole oxidation pathway, Chemical Engineering Journal, 274 (2015) 290-297.

[41] V. Schmalz, T. Dittmar, D. Haaken, E. Worch, Electrochemical disinfection of biologically treated wastewater from small treatment systems by using boron-doped diamond (BDD) electrodes – Contribution for direct reuse of domestic wastewater, Water Research, 43 (2009) 5260-5266.

[42] M. Chen, W. Chu, Photocatalytic degradation and decomposition mechanism of fluoroquinolones norfloxacin over bismuth tungstate: Experiment and mathematic model, Applied Catalysis B-Environmental, 168 (2015) 175-182.

[43] Y.R. Wang, W. Chu, Photo-assisted degradation of 2,4,5-trichlorophenoxyacetic acid by Fe(II)-catalyzed activation of Oxone process: The role of UV irradiation, reaction mechanism and mineralization, Applied Catalysis B-Environmental, 123 (2012) 151-161.

[44] M. Amjadi, J.L. Manzoori, T. Hallaj, A novel chemiluminescence method for determination of bisphenol Abased on the carbon dot-enhanced –H_2O_2 system, Journal of Luminescence, 158 (2015) 160-164.

[45] A. Bianco Prevot, C. Baiocchi, M.C. Brussino, E. Pramauro, P. Savarino, V. Augugliaro, G. Marcì, L. Palmisano, Photocatalytic Degradation of Acid Blue 80 in Aqueous Solutions Containing TiO_2 Suspensions, Environmental Science & Technology, 35 (2001) 971-976.

[46] C.-H. Liao, S.-F. Kang, F.-A. Wu, Hydroxyl radical scavenging role of chloride and bicarbonate ions in the H_2O_2/UV process, Chemosphere, 44 (2001) 1193-1200.

[47] M.L. Alegre, M. Geronés, J.A. Rosso, S.G. Bertolotti, A.M. Braun, D.O. Mártire, M.C. Gonzalez, Kinetic Study of the Reactions of Chlorine Atoms and $Cl_2^{\bullet-}$ Radical Anions in Aqueous Solutions. 1.

Reaction with Benzene, The Journal of Physical Chemistry A, 104 (2000) 3117-3125.
[48] M.J. Watts, K.G. Linden, Chlorine photolysis and subsequent OH radical production during UV treatment of chlorinated water, Water Research, 41 (2007) 2871-2878.
[49] T. An, H. Yang, W. Song, G. Li, H. Luo, W.J. Cooper, Mechanistic Considerations for the Advanced Oxidation Treatment of Fluoroquinolone Pharmaceutical Compounds using TiO_2 Heterogeneous Catalysis, The Journal of Physical Chemistry A, 114 (2010) 2569-2575.
[50] T. An, H. Yang, G. Li, W. Song, W.J. Cooper, X. Nie, Kinetics and mechanism of advanced oxidation processes (AOPs) in degradation of ciprofloxacin in water, Applied Catalysis B: Environmental, 94 (2010) 288-294.
[51] S. Babić, M. Periša, I. Škorić, Photolytic degradation of norfloxacin, enrofloxacin and ciprofloxacin in various aqueous media, Chemosphere, 91 (2013) 1635-1642.
[52] A.S. Giri, A.K. Golder, Ciprofloxacin degradation from aqueous solution by Fenton oxidation: reaction kinetics and degradation mechanisms, Rsc Advances, 4 (2014) 6738-6745.
[53] M.A. Oturan, J. Peiroten, P. Chartrin, A.J. Acher, Complete Destruction of p-Nitrophenol in Aqueous Medium by Electro-Fenton Method, Environmental Science & Technology, 34 (2000) 3474-3479.

Figures and Tables Caption

Figure 1. (a) CIP decay by different catalysts and sole-SSL; (b) UV–visible diffuse reflectance spectra of the as-prepared samples; (c) DMPO-ESR spin-trapping spectra for ·OH radicals; (d) TEM image of $Bi_2O_3/(BiO)_2CO_3$ heterojunction

Experiment Conditions for CIP decay in Figure 1a: $[CIP]_0$ = 10 mg/L, $[Catalyst]_0$ = 0.5 g/L at neutral pH under simulated solar light irradiation

Figure 2. Effect of $[CIP]_0$.

Experiment conditions: $[Bi_2O_3/(BiO)_2CO_3]_0$ = 0.5 g/L at neutral pH under simulated solar light irradiation

Figure 3. Effect of $[Bi_2O_3/(BiO)_2CO_3]_0$.

Experiment Conditions: $[CIP]_0$ = 10 mg/L at neutral pH under simulated solar light

Figure 4. Effect of pH.

Experiment Conditions: $[CIP]_0$ = 10 mg/L, $[Bi_2O_3/(BiO)_2CO_3]_0$ = 0.5 g/L, solar light irradiation

Figure 5. Zeta potential of $Bi_2O_3/(BiO)_2CO_3$.

Figure 6. Comparison between the experimental data and the predicted results from the proposed models for the CIP decay in the SSL-$Bi_2O_3/(BiO)_2CO_3$ process.

Experiment conditions:

A: $[Bi_2O_3/(BiO)_2CO_3]_0$ = 0, $[CIP]_0$ = 10 g/L, pH = 5.5;

B: $[Bi_2O_3/(BiO)_2CO_3]_0$ = 0.5 g/L, $[CIP]_0$ = 10 g/L, pH = 5.5;

C: $[Bi_2O_3/(BiO)_2CO_3]_0$ = 0.5 g/L, $[CIP]_0$ = 5 g/L, pH = 5.5;

D: $[Bi_2O_3/(BiO)_2CO_3]_0$ = 0.5 g/L, $[CIP]_0$ = 5 g/L, pH = 5.9

Figure 7. Effect of anions.

Experiment Conditions: $[CIP]_0$ = 10 mg/L, $[Bi_2O_3/(BiO)_2CO_3]_0$ = 0.5 g/L, $[anion]_0$ = 10 mM, at neutral pH under the simulated solar light irradiation

Figure 8. Accumulation profiles of CIP, intermediates

Experiment Conditions: $[CIP]_0$ = 1 mM, $[Bi_2O_3/(BiO)_2CO_3]_0$ = 0.5 g/L, at neutral pH under simulated solar light irradiation

Figure 9. The proposed pathways for CIP decay.

Figure 10. Accumulation profiles of inorganic ions

Experiment Conditions: $[CIP]_0$ = 1 mM, $[Bi_2O_3/(BiO)_2CO_3]_0$ = 0.5 g/L at neutral pH under the

simulated solar light irradiation.

Figure 11. The toxicity, TOC and CIP at different reaction times

Experiment Conditions: $[CIP]_0$ *= 1 mM,* $[Bi_2O_3/(BiO)_2CO_3]_0$ *= 0.5 g/L, at neutral pH under simulated solar light irradiation, Escherichia coli dosage = 50μL at* 1×10^5 *cfu/mL*

Table 1. Properties of catalysts.

Table 2. Frontier electron densities on the atoms of FLU molecule calculated by Gaussian 09 program at the B3LYP/6-311G** level

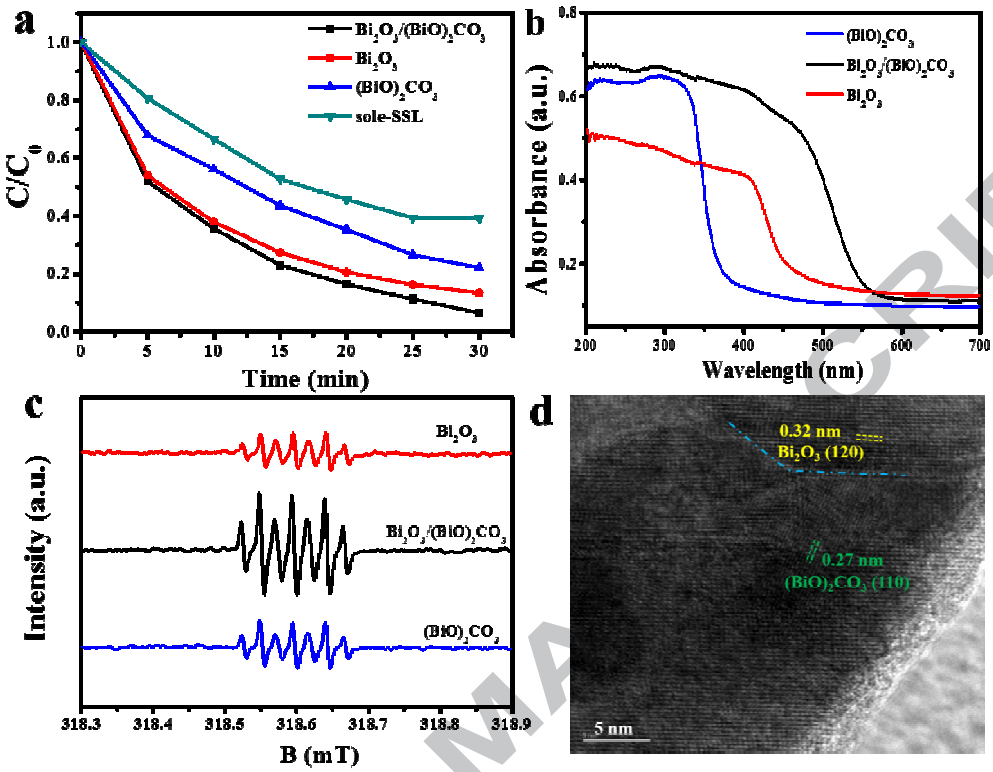

Figure 1. (a) CIP decay by different catalysts and sole-SSL; (b) UV–visible diffuse reflectance spectra of the as-prepared samples; (c) DMPO-ESR spin-trapping spectra for ·OH radicals; (d) TEM image of $Bi_2O_3/(BiO)_2CO_3$ heterojunction

Experiment Conditions for CIP decay in Figure 1a: $[CIP]_0$ = 10 mg/L, $[Catalyst]_0$ = 0.5 g/L at neutral pH under simulated solar light irradiation

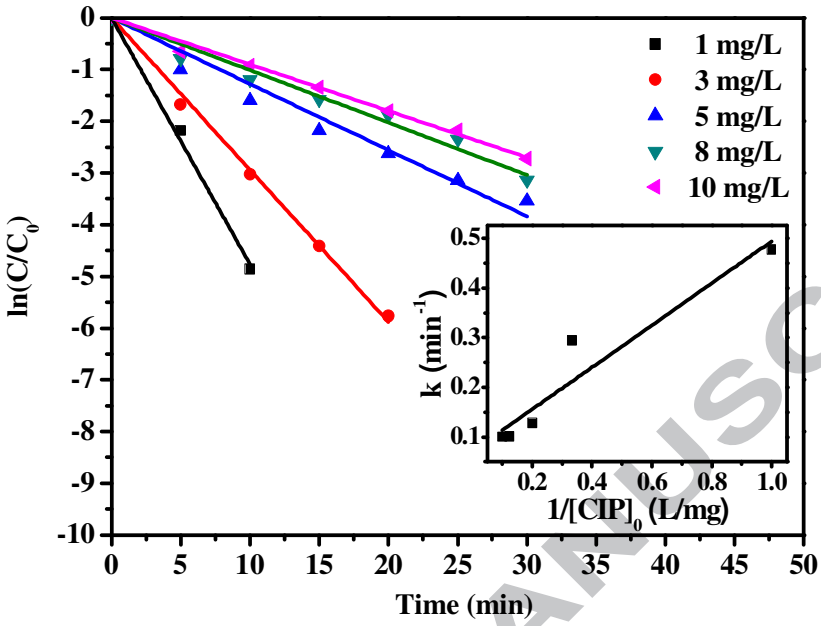

Figure 2. Effect of $[CIP]_0$

Experiment conditions: $[Bi_2O_3/(BiO)_2CO_3]_0$ *= 0.5 g/L at neutral pH under simulated solar light irradiation*

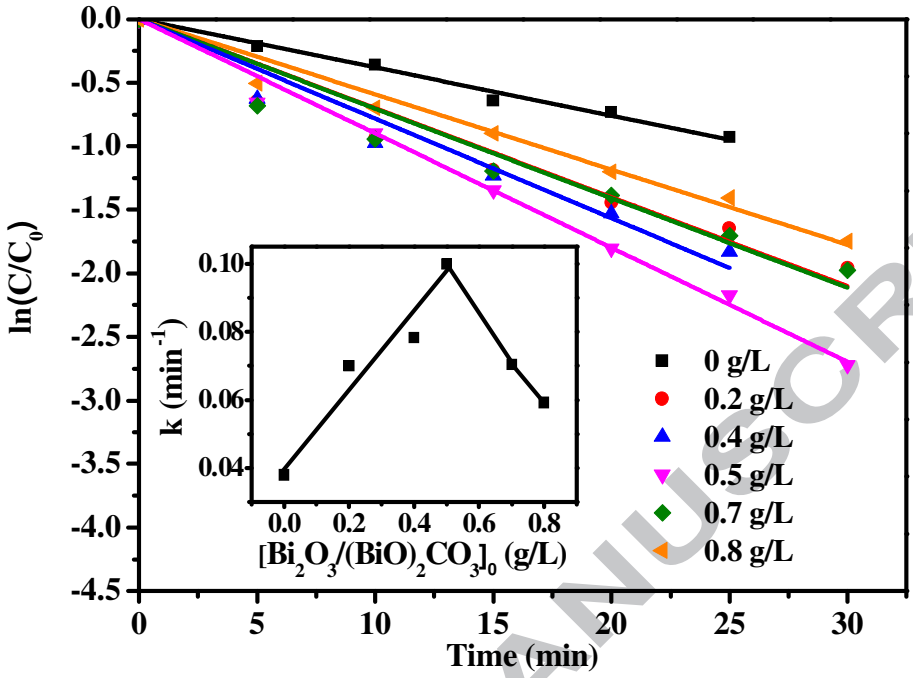

Figure 3. Effect of $[Bi_2O_3/(BiO)_2CO_3]_0$

Experiment Conditions: $[CIP]_0$ = 10 mg/L at neutral pH under simulated solar light irradiation

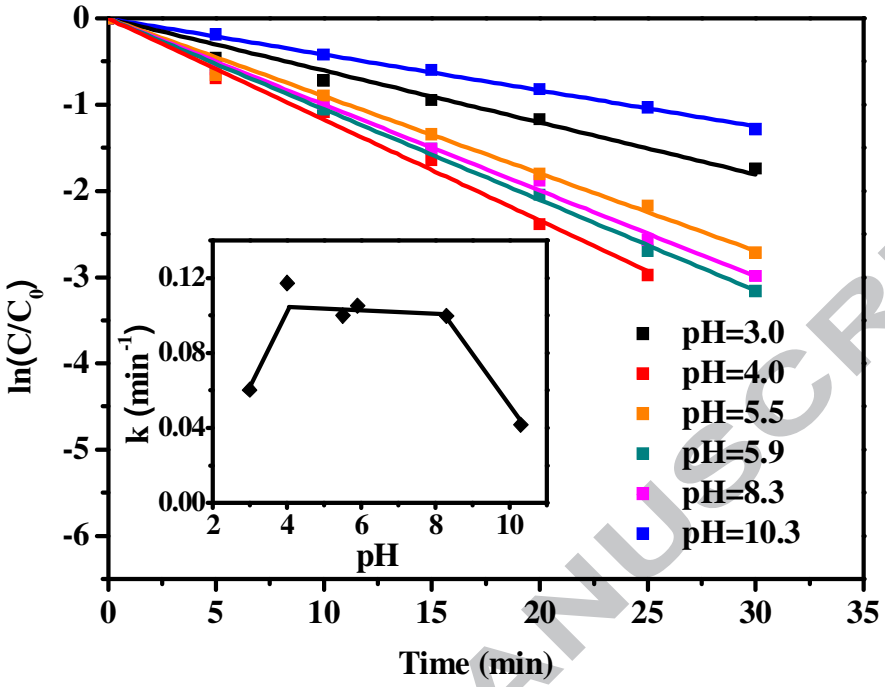

Figure 4. Effect of pH

Experiment Conditions: $[CIP]_0$ = 10 mg/L, $[Bi_2O_3/(BiO)_2CO_3]_0$ = 0.5 g/L, solar light irradiation

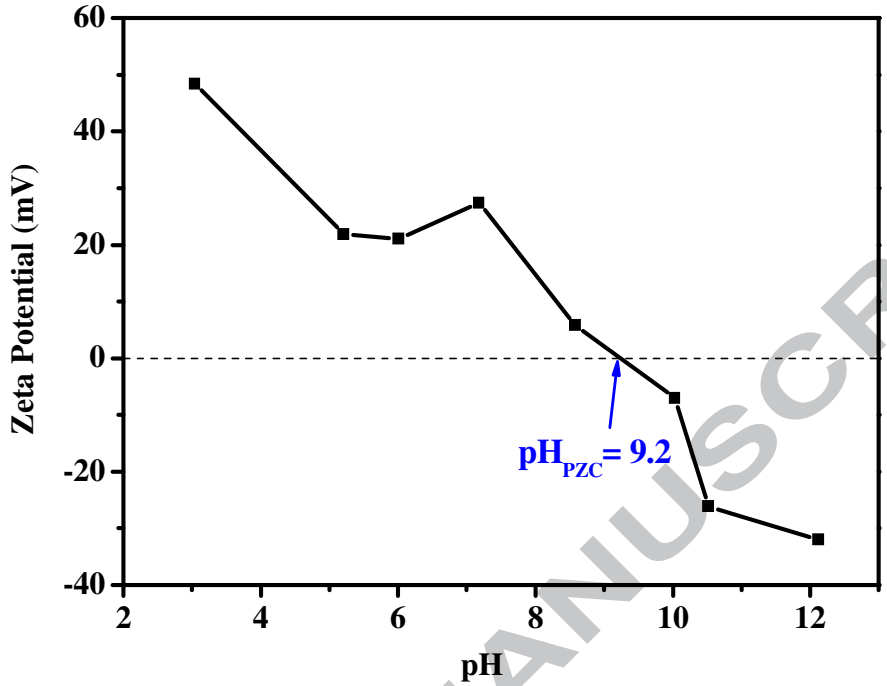

Figure 5. Zeta potential of $Bi_2O_3/(BiO)_2CO_3$

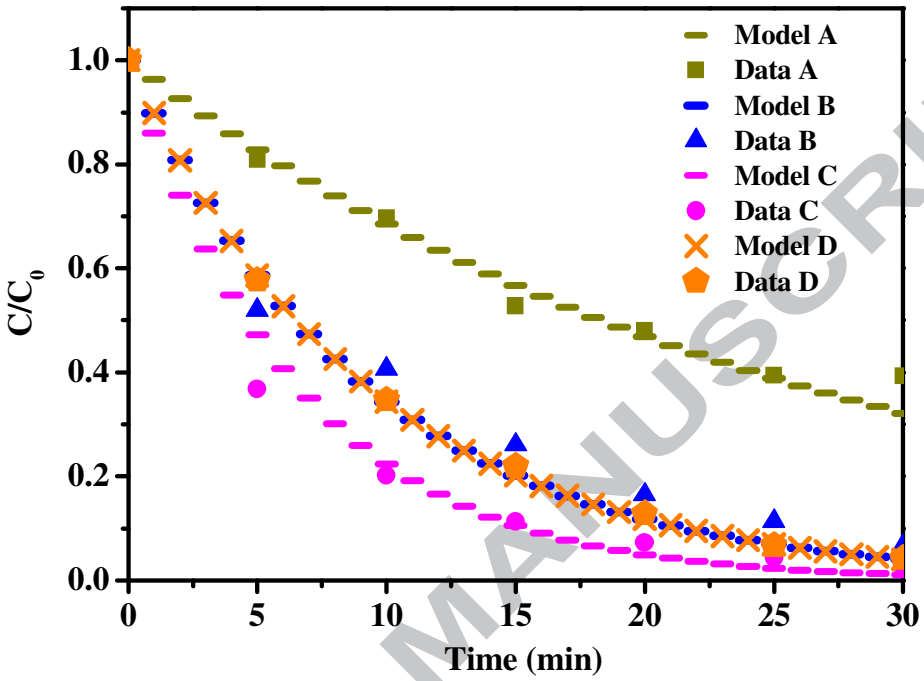

Figure 6. Comparison between the experimental data and the predicted results from the proposed models for the CIP decay in the SSL-Bi_2O_3/$(BiO)_2CO_3$ system

Experiment conditions:

A: $[Bi_2O_3/(BiO)_2CO_3]_0$ = 0, $[CIP]_0$ = 10 g/L, pH = 5.5;

B: $[Bi_2O_3/(BiO)_2CO_3]_0$ = 0.5 g/L, $[CIP]_0$ = 10 g/L, pH = 5.5;

C: $[Bi_2O_3/(BiO)_2CO_3]_0$ = 0.5 g/L, $[CIP]_0$ = 5 g/L, pH = 5.5;

D: $[Bi_2O_3/(BiO)_2CO_3]_0$ = 0.5 g/L, $[CIP]_0$ = 5 g/L, pH = 5.9

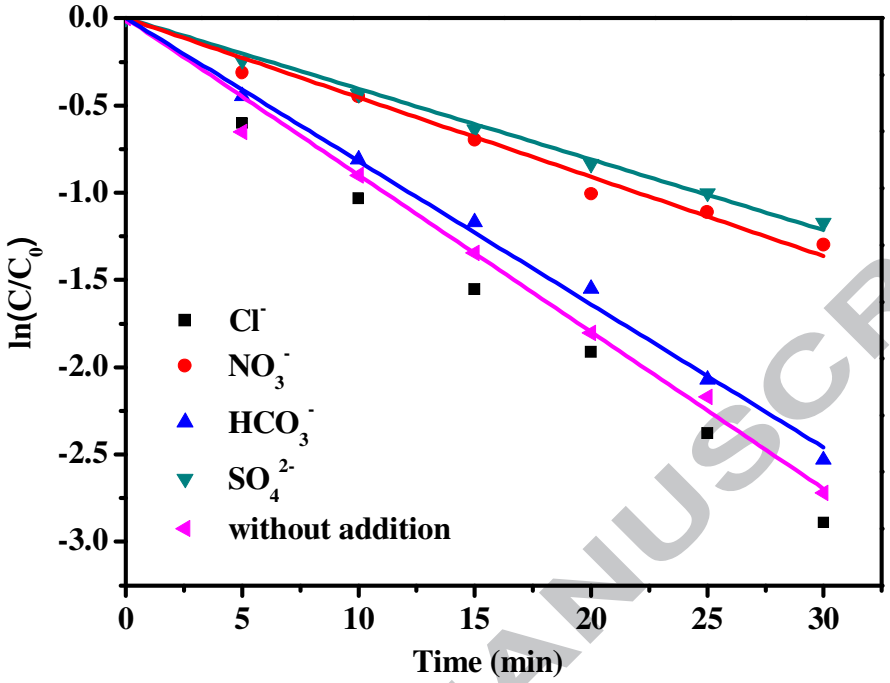

Figure 7. Effect of anions

Experiment Conditions: $[CIP]_0$ = 10 mg/L, =$[Bi_2O_3/(BiO)_2CO_3]_0$ = 0.5 g/L, $[anion]_0$ = 10 mM, at neutral pH under the simulated solar light irradiation

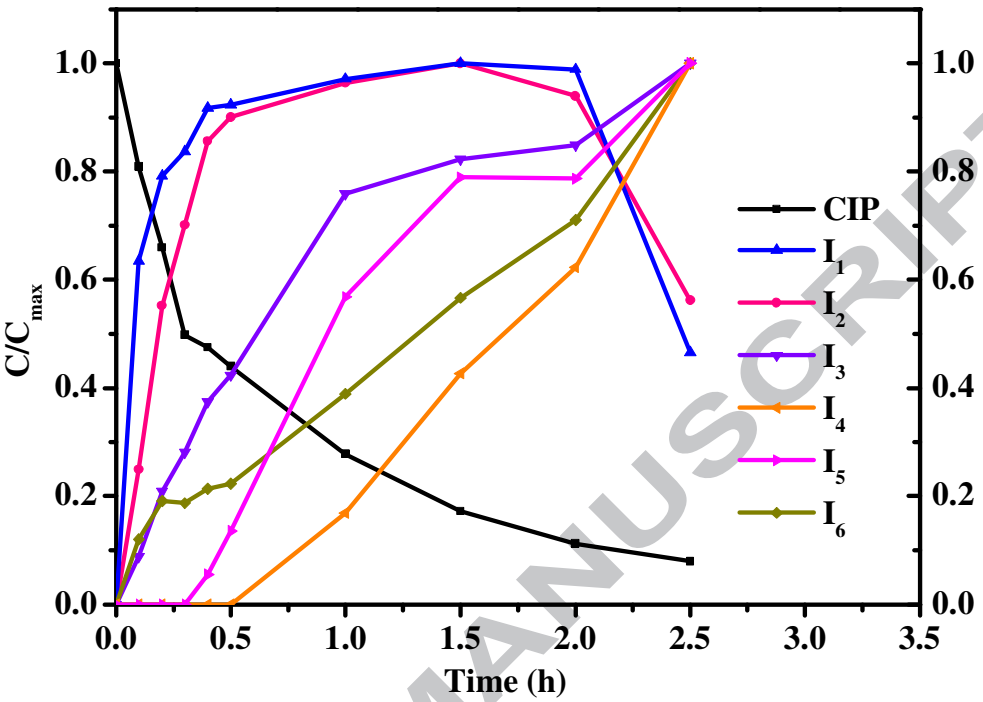

Figure 8. Accumulation profiles of CIP and intermediates

Experiment Conditions: $[CIP]_0$ = 1 mM, $[Bi_2O_3/(BiO)_2CO_3]_0$ = 0.5 g/L, at neutral pH under simulated solar light irradiation

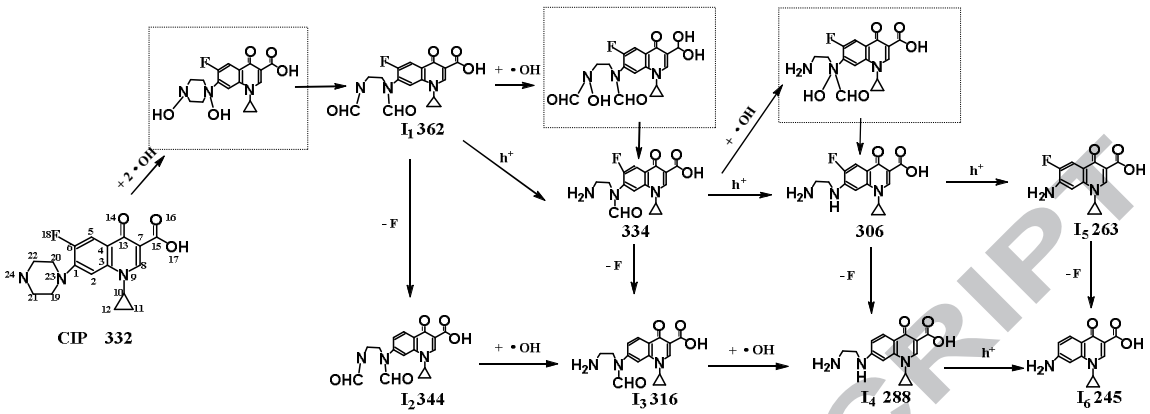

Figure 9. The proposed pathways for CIP decay

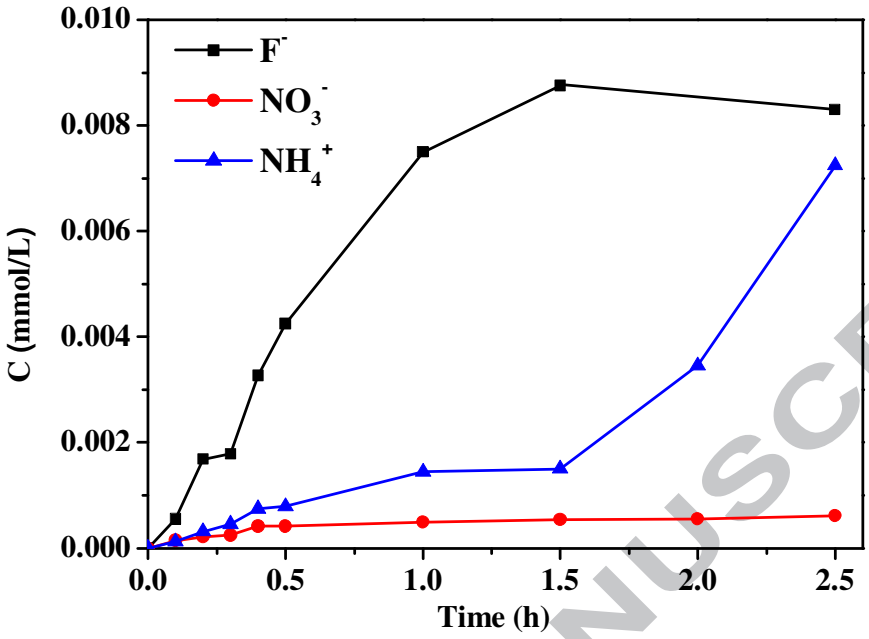

Figure 10. Accumulation profiles of inorganic ions

Experiment Conditions: $[CIP]_0$ = 1 mM, $[Bi_2O_3/(BiO)_2CO_3]_0$ = 0.5 g/L at neutral pH under the simulated solar light irradiation.

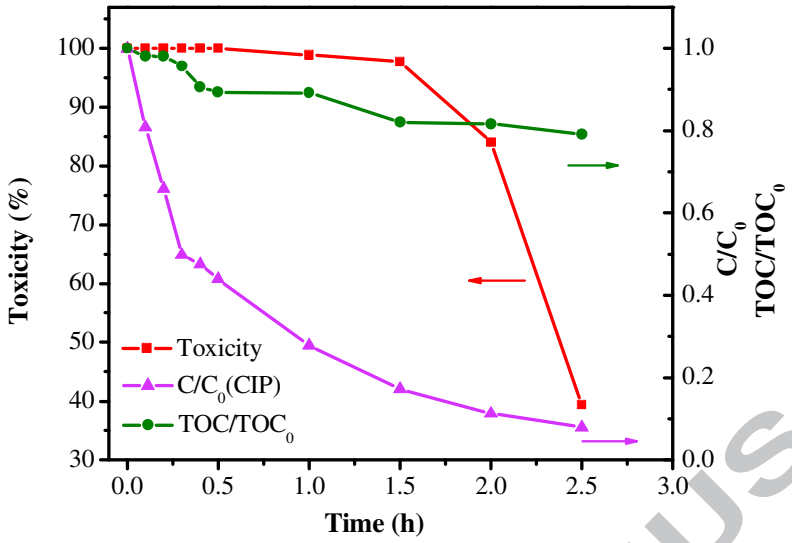

Figure 11. The toxicity, TOC and CIP at different reaction times

Experiment Conditions: $[CIP]_0$ *= 1 mM,* $[Bi_2O_3/(BiO)_2CO_3]_0$ *= 0.5 g/L, at neutral pH under simulated solar light irradiation, Escherichia coli dosage = 50 µL at* 1×10^5 *cfu/mL*

Table 1. Properties of catalysts

	$Bi_2O_3/(BiO)_2CO_3$	$(BiO)_2CO_3$	Bi_2O_3
Surface Area(m^2/g)	4.32	1.93	0.66
Effective Diameter (nm)	19.28	269.4	115.8

Table 2. Frontier electron densities on the atoms of FLU molecule calculated by Gaussian 09 program at the B3LYP/6-311G** level

Atom (number)	$2FED^2_{HOMO}$	$FED^2_{HOMO} + FED^2_{LUMO}$	Atom (number)	$2FED^2_{HOMO}$	$FED^2_{HOMO} + FED^2_{LUMO}$
C (1)	0.090621	0.158258	C (13)	0.00161	0.108626
C (2)	0.025205	0.146887	O (14)	0.004133	0.103079
C (3)	0.01972	0.012854	C (15)	0.000163	0.001152
C (4)	0.038335	0.048684	O (16)	0.000406	0.000679
C (5)	0.078313	0.193792	O (17)	9.5E-05	0.000241
C (6)	0.079633	0.06241	F (18)	0.006405	0.006216
C (7)	0.002533	0.010849	C (19)	0.077058	0.051349
C (8)	0.000983	0.171663	C (20)	0.077052	0.051335
N (9)	0.002714	0.090949	C (21)	0.053052	0.035217
C (10)	0.001546	0.001115	C (22)	0.053057	0.035216
C (11)	4.23E-05	0.007639	N (23)	0.496292	0.24867
C (12)	4.22E-05	0.007621	N (24)	0.890989	0.445498

Highlights

- $Bi_2O_3/(BiO)_2CO_3$ heterojunction was superior than the pristine components;
- Kinetics model in terms of operating parameters fitted well to experimental data;
- Inorganic anions had a different degree of influence on the CIP decay efficiency;
- The decay mechanism was proposed by both experiment and theoretical calculation.
- Efficient alleviation on TOC and toxicity were obtained.

Graphical Abstract